Radiology: Cardiothoracic Imaging

Dual-Energy CT Pulmonary Angiography (DECTPA) Quantifies Vasculopathy in Severe COVID-19 Pneumonia

Carole A Ridge FFRRCSI[1]*, Sujal R Desai MD FRCP FRCR[1]*, Nidhish Jeyin BSc[2], Ciara Mahon MRCPI[1], Dione L Lother MB BCh[1], Saeed Mirsadraee MD PhD MRCS FRCPE FRCR[1], Tom Semple FFR[1], Susanna Price FRCP FESC FFICM PhD [3], Caroline Bleakley MD MRCP[3], Deepa J Arachchillage MRCP FRCPath MD [4], Elizabeth Shaw MSc[1], Brijesh V Patel MRCP FRCA FFICM PhD [3], Simon PG Padley BSc MBBS FRCP FRCR [1], Anand Devaraj MD MRCP FRCR [1]

*Joint First Authors (equal contribution)

Affiliation:
[1]Department of Imaging, Royal Brompton Hospital, London, UK
[2]Imperial College London, London, UK
[3]Anaesthesia and Critical Care, Royal Brompton Hospital, London, UK,
[4] Department of Haematology, Imperial College London, London, UK and Department of Haematology, Royal Brompton Hospital, London, UK

Corresponding Author:
Carole A Ridge, Department of Imaging, Royal Brompton Hospital, London, UK
Email: c.ridge@rbht.nhs.uk

Key Points

Perfusion defects on DECTPA perfused blood volume maps are common in patients with severe COVID-19 pneumonia, even in the absence of pulmonary thrombosis.

Quantitative pulmonary relative perfused blood volume (PBV/PAenh) correlated with disease duration ($p = 0.04$), and negatively with right ventricular dysfunction ($p = 0.001$), independent of age, gender, body mass index and ethnicity.

Summary Statement

Significantly decreased (qualitative and quantitative) lung enhancement on dual-energy CT pulmonary angiography is an early feature of severe COVID-19 pneumonia and is associated with right ventricular dysfunction.

ABSTRACT

Background: The role of dual energy computed tomographic pulmonary angiography (DECTPA) in revealing vasculopathy in coronavirus disease 2019 (COVID-19) has not been fully explored.

Purpose: To evaluate the relationship between DECTPA and disease duration, right ventricular dysfunction (RVD), lung compliance, D-dimer and obstruction index in COVID-19 pneumonia.

Materials and Methods: This institutional review board approved this retrospective study, and waived the informed consent requirement. Between March-May 2020, 27 consecutive ventilated patients with severe COVID-19 pneumonia underwent DECTPA to diagnose pulmonary thrombus (PT); 11 underwent surveillance DECTPA 14 ±11.6 days later. Qualitative and quantitative analysis of perfused blood volume (PBV) maps recorded: i) perfusion defect 'pattern' (wedge-shaped, mottled or amorphous), ii) presence of PT and CT obstruction index (CTOI) and iii) PBV relative to pulmonary artery enhancement (PBV/PAenh); PBV/PAenh was also compared with seven healthy volunteers and correlated with D-Dimer and CTOI.

Results: Amorphous (n=21), mottled (n=4), and wedge-shaped (n=2) perfusion defects were observed (M=20; mean age=56 ±8.7 years). Mean extent of perfusion defects=36.1%±17.2. Acute PT was present in 11/27(40.7%) patients. Only wedge-shaped defects corresponded with PT (2/27, 7.4%). Mean CTOI was 2.6±5.4 out of 40. PBV/PAenh (18.2 ±4.2%) was lower than in healthy volunteers (27 ±13.9%, $p = 0.002$). PBV/PAenh correlated with disease duration ($\beta = 0.13$, $p = 0.04$), and inversely correlated with RVD ($\beta = -7.2$, $p = 0.001$), persisting after controlling for confounders. There were no linkages between PBV/PAenh and D-dimer or CTOI.

Conclusion: Perfusion defects and decreased PBV/PAenh are prevalent in severe COVID-19 pneumonia. PBV/PAenh correlates with disease duration and inversely correlates with RVD. PBV/PAenh may be an important marker of vasculopathy in severe COVID-19 pneumonia even in the absence of arterial thrombus.

INTRODUCTION

Severe acute respiratory failure is the dominant cause of death in patients with coronavirus disease 2019 (COVID-19) (1). The pathophysiology and imaging features of severe COVID-19 pneumonia have been the focus of considerable interest from the outset of the pandemic. In early disease, widespread ground-glass opacification predominates on thoracic computed tomography (CT) (2-6), and is supposedly associated with highly compliant lungs and disrupted vasoregulation, (7). Vascular dysregulation is believed to be consequence of exaggerated activation of inflammatory and coagulation cascades (termed 'immunothrombosis') (1, 8-12). Later in the course of disease, CT more commonly shows consolidation and fibrosis associated with lower lung compliance (13).

There is growing evidence from radiologic and pathologic studies of a significant vasculopathy in COVID-19 pneumonia (14-17): in a recent study of post-mortem lungs in COVID-19, there were widespread microthromboses and striking new vessel formation (16). Furthermore, based on *qualitative* analyses, a number of studies have highlighted the potential role of dual energy computed tomography pulmonary angiography (DECTPA) (15, 18-21). Accordingly, in the present study we aimed to evaluate the relationships between a *quantitative* measure of perfusion on DECTPA (relative perfused blood volume, PBV/PAenh) (22), and i) disease duration, ii) right ventricular dysfunction on echocardiography iii) D-dimer levels and (iv) obstruction score (23) in patients with severe COVID-19 pneumonia. A secondary aim was to compare PBV/PAenh in COVID-19 pneumonia to that of normal volunteers.

MATERIALS & METHODS

Study Design

This retrospective, observational study was approved by United Kingdom Health Research Authority (HRA), through the integrated research application system (IRAS # 265630); the need for informed consent was waived. No industry financial support was given to the authors, who had control of the data and the information submitted for publication at all times. Twenty seven consecutive patients (20 men, mean age 53.4 years (range, 24-70); 7 women, mean age 60.4 years (range, 54-66) were transferred to the Royal Brompton Hospital, United Kingdom — a national tertiary referral centre for patients with severe acute respiratory failure (SARF) — between March 21st and May 24th, 2020. Included patients were i) mechanically ventilated and ii) imaged with DECTPA to diagnose potential pulmonary thrombus (PT) (Figure 1). Patients on extracorporeal membrane oxygenation (ECMO) support were excluded given the potential confounding factor of contrast egress through the return ECMO cannula. Patients with a body mass index greater than 35kg/m^2, and those with an inability to arm-raise above the head (to mitigate beam-hardening artifact) were excluded. Q*ualitative* DETCPA findings in a subset of 18 patients with COVID-19 pneumonia have been previously reported (15). This early data demonstrated perfusion defects on perfused blood volume (PBV) maps, when available, as well as the presence of vascular dilatation on conventional CT, hypercoagulability and an increased dead space in 39 patients suggesting that pulmonary angiopathy was accountable for hypoxia observed in patients requiring mechanical ventilation for severe COVID-19 pneumonia. This provided the impetus for the further *quantitative* study.

Clinical Investigations

The diagnosis of severe acute respiratory syndrome-coronavirus-2 (SARS-CoV-2) infection was confirmed on real-time reverse transcriptase polymerase chain reaction assay in all patients. The date of symptom onset was documented from clinical notes. Treating physicians determined the type and frequency of investigations in accordance with standard institutional practice. The results of the following investigations, performed within a maximum of 48 hours prior to DECTPA, were recorded: i) D-dimer levels; and ii) right ventricular dysfunction on transthoracic echocardiography, recorded as a binary variable of 'normal' or 'abnormal' with the latter graded as mild, moderate or severe right ventricular

dysfunction. Dynamic lung compliance and positive end expiratory pressure (PEEP) were measured by the mechanical ventilator within 4 hours of DECTPA.

Dual-Energy CT Scanning Protocol and Image Reconstruction

Scanning methodology are provided in detail in the Supplementary Data. All DECTPA studies were acquired on a dedicated dual-source machine (Siemens FLASH, Siemens Healthineers, Forcheim, Germany). Images were acquired at a trigger of 120 HU using bolus tracking at the main pulmonary artery (PA), when available (n=26 DECTPA studies); to document contrast dynamics in each patient, the rate of PA enhancement was recorded in HU/second using bolus tracking CT images. The iodine content of each voxel was derived using a three-material-decomposition algorithm for air, soft-tissue, and iodine (23) and reconstructed using a "dense lung" PBV map with a maximum threshold of -200 Hounsfield units (HU). The upper threshold of -200 HU was identified as a cutoff, which included the typical ground glass opacity seen in viral pneumonia. This threshold applied only to qualitatively assessed PBV images, and not quantitative measurements, which included both aerated and non-aerated lung.

Qualitative DECTPA Analysis

PBV images were reviewed in consensus by two thoracic radiologists (CAR and SPGP) with 14- and 30-years' experience, respectively, blinded to all clinical data using dual energy processing software (Syngo Via Dual Energy, Siemens Healthineers, Forcheim, Germany). A perfusion defect was defined as a segmental (25) region of hypoenhancement using an automatically generated colour scale. The proportion of aerated lung affected by perfusion defects was visually estimated as a percentage of both lungs. In cases of uncertainty, readers had the ability to measure PBV/PAenh, a threshold of < 20% was categorised as representing hypoperfusion (26). The 'morphology' of perfusion defects was categorised as i) wedge-shaped (analogous to the appearance seen in patients with acute pulmonary embolism (PE) (27), ii) mottled (as seen in idiopathic or chronic thromboembolic pulmonary hypertension (28) or iii) amorphous (Figure 2). The pulmonary arterial tree was assessed to determine the presence of PT, the order of involvement (the main PA representing the "first order" artery) and if the predominant perfusion defect pattern was attributable to PT in a corresponding anatomical distribution.

Quantitative DECTPA Analysis

PBV maps were adjusted for arterial opacification by drawing a 1cm^2 region of interest (ROI) over the main PA in transaxial section. The mean "overlay value" of the ROI representing calculated iodine density in mg/ml was acquired by manually creating a ROI around the perimeter of the right and left lungs at the midpoint of each lung in the axial, coronal and sagittal planes (Figure 3), producing the parameters of iodine density in mg/ml and average PBV/PAenh (iodine density in the ROI divided by iodine density in the PA, Supplementary Data) (22, 29). Each ROI included aerated and consolidated or atelectatic lung and excluded beam hardening, streak or motion artifacts. PBV/PAenh measurements were acquired by two independent observers, with 1 (NJ) and 14 (CAR) years' experience of quantitative DETCPA analysis, after completing a training dataset of 10 DECTPA. The average of 6 multiplanar measurements (three planes in each lung) was used for correlation with clinical findings (Figure 3). To establish the range of normal values, PBV/PAenh was calculated in a cohort of 7 normal volunteers (4 men, mean age 51.7±22.8 years; 3 women, mean age 32.6±19.3 years) recruited in a previously published case control study using the same image acquisition, CT scanner and analysis methods (30) (Supplementary Table *1*).

Statistical Analysis

Data was analyzed using SPSS (IBM Corp, Released 2019, IBM SPSS Statistics for Mac, Version 25.0, Armonk). Descriptive statistics are given as means (± standard deviations) or frequency and percentage, as appropriate. As clinical investigations were matched to the time of scanning and varied over time, they are reported on a per-scan basis. The relationship between quantitative and qualitative analysis and clinical investigations was investigated for the initial DECTPA. Independent sample t-tests were used to evaluate for differences in continuous variables. The dependent variable of interest showed normal distribution based on the Shapiro-Wilk test. Chi-square tests were used to analyze the differences in categorical variables. Both univariate and multivariate linear regression was used to analyze for associations between variables and a continuous, independent variable. Univariate and multivariate logistic regression analyzed the relationship between variables and a dichotomous independent variable. Inter-class correlation was used to test reader agreement using a two way ANOVA calculation. Statistical measures were considered statistically significant at a p-value of 0.05 or less.

RESULTS

Baseline Demographic and Clinical Characteristics

Between March 21 to May 24, 2020, 27 mechanically-ventilated patients (20 men, mean age 53.4 years (range, 24-70); 7 women, mean age 60.4 years (range, 54-66)) with SARF underwent DECTPA (11 patients had repeat surveillance DECTPA). Patient demographic and clinical characteristics are shown in Tables 1 and 2. The mean symptom duration prior to DECTPA was 11.5 ±7.1 days. Diabetes mellitus, hypertension and a BMI>25kg/m^2 were a feature in 7/27(25.9%), 12/27 (44.4%), 21/27 (77.7%) of patients respectively.

Of the 27 patients studied, 20 were intubated prior to transfer from another institution at an average of 2.8 ±3.9 days prior to admission whereas seven were intubated and mechanically-ventilated following admission to our institution. Four patients were self-ventilating through a tracheostomy at the time of surveillance CT, and therefore ventilatory measurements were not available. Mean dynamic compliance was reduced (32.9±19.1 ml/cmH2O) and abnormal at the time of CT in 29/34 (85.3%). Mean PEEP was 10±2.7cm H_20.

Baseline DECTPA Findings in COVID-19 and Comparison with Normal Volunteers

Arterial filling defects, consistent with PT, were present on ten initial and six surveillance DECTPA, with only one new PT identified on surveillance DECTPA. Thus, overall, PT was present in 11 patients; thromboses were seen in second order (n=2), third order (n=2), fourth order (n=3) and fifth order (n=4) arteries.

Visually-scored perfusion defects (Figure 2) were present in 38/38 (100%) DECTPA studies, with a mean extent of 36.1±17.2% (Table 3). At initial CT, perfusion defects were classified as wedge-shaped (n = 2), mottled (n = 4) and amorphous (n =21) (Figure 2). Qualitative analysis attributed the *predominant* pattern of perfusion defect to PE in only 2 of 27 patients, both of whom had wedge shaped perfusion defects. The mean Qanadli CT obstruction index was 2.6±5.4 out of a maximum score of 40.

Quantitative analysis revealed an average PBV/PAenh of 17.5±4.4% at initial DECTPA and 19.8±3.4% on surveillance DECTPA (p=0.008). PBV/PAenh values were significantly lower than for seven normal volunteers (average PBV/PAenh 27±13.9% (p=0.002) (Table 1, supplementary material). No normal volunteer DECTPA studies demonstrated perfusion defects. Average iodine density was 2.3 ±0.7mg/ml at initial DECTPA and 2.6 ±0.6mg/ml on surveillance DECTPA (p=0.7). There was no statistically significant difference in iodine density compared to normal volunteers (2.5, p = 0.7). Interclass correlation (ICC) for PBV/PAenh measurements was excellent (ICC=0.861, 95% confidence interval 0.733-0.928, p < 0.0001).

Relationship Between DECTPA Variables, Right Ventricular Function, D-dimer Levels and Obstruction Score in COVID-19 Pneumonia

The clinical and laboratory findings at the time of initial DECTPA are shown in Table 2. Right ventricular function was abnormal in 33/39 (84.7%) patients and graded mild (n= 13), moderate (n = 12) and severe (n=8). There was no relationship between the rate of enhancement (mean 20±9HU/s) in the main PA and right ventricular dysfunction (p=0.46). The mean D-dimer level, abnormal in all patients, was 5500.05±8691.15 ng/ml. On linear regression analysis, there was an inverse relationship between PBV/PAenh on initial DECTPA and right ventricular dysfunction (β = -7.2, SE 1.9, p = 0.001), which remained significant after controlling for age, gender, BMI and ethnicity (β = -5.6, SE 1.6, p = 0.001). When RV dysfunction was subdivided into mild, moderate and severe grades, the statistical significance of this relationship was not maintained, potentially due to small sample size. There was no statistically significant relationship between D-dimer levels or Qanadli obstruction index and qualitative or quantitative DECTPA variables.

Relationship Between DECTPA Variables, Disease Duration and Ventilator Measurements in COVID-19 Pneumonia

The mean interval between symptom onset and initial DECTPA was 11.5±7.1 days. Surveillance DECTPA was acquired at an average of 14.0±11.6 days after the initial DECTPA (Figure 4). On linear regression analysis there was no statistically significant correlation between the average perfusion defect extent and duration of disease. However, when a binary time interval of <14 days was applied, the extent of visually scored perfusion defect was greater on DECTPA performed within 14 days of symptom onset compared to those performed after this time point (extent of perfusion defect of 40.6% compared to 26.3% after 14 days, $p = 0.049$).

On linear regression analysis there was a positive correlation between PBV/PAenh and duration of disease ($\beta = 0.13$, SE 0.64, $p = 0.04$) and, on multivariate linear regression, this remained significant after controlling for age, gender, BMI and ethnicity ($\beta = 0.156$, SE .062, $p = 0.017$). There was an inverse relationship between PBV/PAenh and dynamic lung compliance ($\beta = -18.5$, SE 7.6, $p = 0.02$) which, again on multivariate linear regression, remained significant after controlling for age, gender, BMI and ethnicity ($\beta = -0.118$, SE 0.034, $p = 0.002$). There was no statistically significant relationship between PBV/PAenh and PEEP, suggesting that ventilator pressures did not influence iodine distribution.

DISCUSSION

We have shown in this study that pulmonary relative perfused blood volume (PBV/PAenh) — a quantitative marker of lung perfusion — is not only significantly reduced in COVID-19 respiratory failure when compared with normal volunteers but also that there is an independent and inverse relationship with right ventricular dysfunction. Additionally, PBV/PAenh increased with duration of disease suggesting that vascular dysregulation improves with time and that DECTPA might, alongside more traditional physiologic parameters, be utilized as another important marker of disease surveillance.

The qualitative and quantitative analyses in the present study have shown that perfusion defects on DECTPA are prevalent in severe COVID-19 pneumonia. As far as we are aware, this is the first report in which DECTPA scans have been systematically evaluated with quantitative analysis. Perfusion abnormalities were present irrespective of the presence of acute pulmonary emboli. More importantly, Putting the above findings together, DECTPA may reflect microvascular dysregulation, posited as one of the important pathophysiologic abnormalities in early COVID-19 respiratory failure (7). As further support for this 'vasocentric' hypothesis, we have shown that the morphology of perfusion defects was categorized as amorphous in the majority, as opposed to the more typical wedge-shaped peripheral defects seen in acute pulmonary embolism; the amorphous pattern is akin to that observed in idiopathic pulmonary hypertension and chronic thromboembolic pulmonary hypertension (15).

The relationship between PBV/PAenh and disease duration may provide insights into the pathophysiology of COVID-19-related severe respiratory failure. It is hypothesised in the literature that in 'early' COVID-19-induced ARDS, compliance is preserved in the face of poor oxygenation and there is a poor response to high PEEP (7). This has been dubbed the 'type L' physiology, characterized morphologically by a pattern of ground-glass opacification on CT. By contrast, in those with progressive disease, there is then a transition to a physiology that is more in keeping with typical ARDS, namely with lower compliance and higher response to PEEP, termed the 'type H' phenotype. Our observations provide some support for this theory: PBV/PAenh was seen to improve with time in our patients, whereas compliance, although not likely to be related to vasculopathy, decreased with time from

disease onset. This seemingly neat categorization of COVID-19 lung physiology has obvious attractions. However, it seems highly likely that, in individual patients, there will be considerable overlap between the proposed phenotypes.

The observation of decreased compliance over time, may raise the question that it is volume loss due to fibrosis, and not improving perfusion that has given rise to an increased PBV/PAenh in patients imaged later in their disease course, however, we did not observe an increase in iodine density (i.e. concentration) with increasing time from symptom onset, but rather an increase in the relative iodine distribution in the lungs, corrected for opacification of the pulmonary artery (PBV/PAenh). This supports our belief that it is impaired pulmonary perfusion at the outset of the disease, and not loss of volume later in the disease, that is responsible for our observations.

In light of our findings, a brief discussion of right ventricular (RV) dysfunction in COVID-19 is warranted. In one recent study of 100 consecutive patients with COVID-19, there was echocardiographic evidence of RV dysfunction in 32% (31); RV dysfunction was also the most prevalent feature at follow-up. Importantly left ventricular function was preserved in the majority. The progression to right heart failure can manifest as cardiomegaly and right ventricular dilatation in the absence of myocarditis at autopsy in COVID-19 infection (17). No patients in our cohort were diagnosed with myocarditis, leading us to believe that acute cor pulmonale was the most likely culprit (32). Quantitative analysis of DECTPA in our cohort showed that decreasing PBV/PAenh, indicating poorer pulmonary perfusion, is linked with the presence of RV dysfunction, independent of age, sex, BMI or ethnicity. Of note, the rate of enhancement on dynamic bolus-tracking CT images of the PA did not correlate with right ventricular function in this cohort, allaying concerns that the observed decreased PBV/PAenh is simply an artifact of a blunted enhancement curve, as has been observed in pulmonary thromboembolism (22). We believe this is an important finding suggesting, at least in part, that pulmonary vasculopathy may have a direct bearing on cardiac function in COVID-19.

There are obvious limitations in our study. The cohort size is small, and the retrospective methodology introduces potential biases. Another issue is that, in the absence of pathologic proof, causal arguments regarding the true meaning of the radiologic observations must be made with a little caution. However, there is growing consensus of significant vascular pathology in COVID-19 and, given that *biopsy* proof of vascular involvement is impracticable in the majority, we propose that non-invasive imaging biomarkers, such as PBV/PAenh, may be the best indirect marker of vasculopathy. This technique has also been validated by direct comparison with pulmonary blood flow measurement in swine models in the setting of both balloon arterial occlusion and in acute lung injury (33, 34).

A further limitation is the lack of a comparable control group with severe acute respiratory failure without COVID-19 pneumonia. In fact, the preponderance of multiorgan infarction and thrombosis has also been observed in severe acute respiratory syndrome coronavirus (SARS-C0V) (35, 36). This provides the impetus for future study of the utility of DECT in other pulmonary infections. An important technical limitation was that obese patients with a BMI greater than 35 kg/m^2 were not included in this study, due to concerns of image 'noise' and artifactual hypo-enhancement because of contrast egress through the return cannula, respectively; the presence of image noise is particularly problematic in the reconstruction of PBV images. Whilst this might be overcome by increasing exposure factors, it comes with the obvious penalty of an increasing radiation burden. For other technical reasons, patients on ECMO support were also excluded from our analyses. However, in the absence of 'normal' perfusion values for these patients, it was felt that their inclusion would not represent a like-for-like comparison of pulmonary enhancement. The presence of consolidated and atelectatic lung presented a challenge to analysis. This potential confounder was addressed by stipulating that PBV map visual analysis should exclude such portions of lung, as the presence of volume loss may impact the reader's assessment of regional iodine distribution. However, this consolidated or atelectatic lung was included in quantitative analysis, the rationale for this inclusion was that a quantitative comparison of pulmonary iodine over a large ROI compared to pulmonary arterial iodine (PBV/PAenh) was more likely to be accurate than purely visual analysis. A final consideration is that the majority of patients (21/27, 77.8%) in our cohort were therapeutically anticoagulated

(Figure 4), and two of these patients received systemic thrombolysis with the remaining patients receiving prophylactic low molecular weight heparin. As a confounder, this might explain the higher PBV/PAenh later in the course of disease. As future randomized controlled trials are devised, we suggest that DECTPA is used as a surveillance tool, to determine whether the temporal pattern of pulmonary perfusion represents the natural history of the disease, or an anticoagulation-related effect.

In summary, perfusion defects on DECTPA are prevalent in severe COVID-19 pneumonia even in the absence of pulmonary thrombosis; PBV/PAenh is significantly reduced in COVID-19 pneumonia and has an independent inverse relationship with right ventricular dysfunction. PBV/PAenh increases over time suggesting that COVID-19 pulmonary angiopathy may reflect an acute feature of severe COVID-19 pneumonia, which may be utilized as an important marker and surveillance tool.

Acknowledgements

The authors are grateful to the patients and families of those affected by COVID-19 for whom the Royal Brompton Hospital severe acute respiratory failure service had the privilege of delivering care during the pandemic. The images produced for this study would not have been possible without the expertise of the healthcare assistants, nurses, porters, physicists, physicians and radiographers of the Royal Brompton Hospital who showed exemplary dedication in their work. The CT radiography department delivered the highest calibre of imaging under the most challenging circumstances, and for this the authors are in your debt. The authors are also thankful to the Royal Brompton and Harefield Hospitals Charity for financial support in the purchase of dual energy advanced processing software and for statistical analysis performed by Dr Gregory Hanson MD MPH.

References

1. Ruan Q, Yang K, Wang W, Jiang L, Song J. Clinical predictors of mortality due to COVID-19 based on an analysis of data of 150 patients from Wuhan, China. Intensive Care Med. 2020;46(5):846-848.
2. Li Y, Xia L. Coronavirus Disease 2019 (COVID-19): Role of Chest CT in Diagnosis and Management. AJR Am J Roentgenol. 2020;214(6):1280-1286.
3. Gao L, Zhang J. Pulmonary High-Resolution Computed Tomography (HRCT) Findings of Patients with Early-Stage Coronavirus Disease 2019 (COVID-19) in Hangzhou, China. Med Sci Monit. 2020;26:e923885.
4. Huang C, Wang Y, Li X, et al. Clinical features of patients infected with 2019 novel coronavirus in Wuhan, China. Lancet. 2020;395(10223):497-506.
5. Bernheim A, Mei X, Huang M, et al. Chest CT Findings in Coronavirus Disease-19 (COVID-19): Relationship to Duration of Infection. Radiology. 2020;295(3):200463.
6. Pan Y, Guan H, Zhou S, et al. Initial CT findings and temporal changes in patients with the novel coronavirus pneumonia (2019-nCoV): a study of 63 patients in Wuhan, China. Eur Radiol. 2020;30(6):3306-3309.
7. Gattinoni L, Chiumello D, Caironi P, et al. COVID-19 pneumonia: different respiratory treatments for different phenotypes? Intensive Care Med. 2020;1-4.
8. Klok FA, Kruip MJHA, van der Meer NJM, et al. Incidence of thrombotic complications in critically ill ICU patients with COVID-19. Thromb Res. 2020;191:145-147.
9. Chen G, Wu D, Guo W, et al. Clinical and immunological features of severe and moderate coronavirus disease 2019. J Clin Invest. 2020;130(5):2620-2629.
10. Tang N, Li D, Wang X, Sun Z. Abnormal coagulation parameters are associated with poor prognosis in patients with novel coronavirus pneumonia. J Thromb Haemost. 2020;18(4):844-847.
11. Danzi GB, Loffi M, Galeazzi G, Gherbesi E. Acute pulmonary embolism and COVID-19 pneumonia: a random association?. Eur Heart J. 2020;41(19):1858.
12. Xie Y, Wang X,Yang P, Zhang S. COVID-19 Complicated by Acute Pulmonary Embolism. Radiol Cardiothorac Imaging. 2020;2(2):e200067.
13. Liu X, Liu X, Xu Y, et al. Ventilatory Ratio in Hypercapnic Mechanically Ventilated Patients with COVID-19-associated Acute Respiratory Distress Syndrome. Am J Respir Crit Care Med. 2020;201(10):1297-1299.

14. Lang M, Som A, Mendoza DP, et al. Hypoxaemia related to COVID-19: vascular and perfusion abnormalities on dual-energy CT [published online ahead of print, 2020 Apr 30]. Lancet Infect Dis. 2020;S1473-3099(20)30367-4.
15. Patel BV, Arachchillage DJ, Ridge CA et al. Pulmonary angiopathy in severe Covid-19: physiologic, imaging and hematologic observations. Am J Respir Crit Care Med. 2020; (In Press).
16. Ackermann M, Verleden SE, Kuehnel M, et al. Pulmonary Vascular Endothelialitis, Thrombosis, and Angiogenesis in Covid-19 [published online ahead of print, 2020 May 21]. N Engl J Med. 2020;10.1056/NEJMoa2015432.
17. Fox SE, Akmatbekov A, Harbert JL, Li G, Quincy Brown J, Vander Heide RS. Pulmonary and cardiac pathology in African American patients with COVID-19: an autopsy series from New Orleans. Lancet Respir Med. 2020;S2213-2600(20)30243-5.
18. Marsico S, Espallargas Giménez I, Carbullanca Toledo SJ, Del Carpio Bellido LA, Maiques Llácer JM, Zuccarino F. Pulmonary infarction secondary to pulmonary thromboembolism in COVID-19 diagnosed with dual-energy CT pulmonary angiography. Rev Esp Cardiol. 2020;S1885-5857(20)30174-2.
19. Lang M, Som A, Carey D, et al. Radiology: Pulmonary Vascular Manifestations of COVID-19 Pneumonia. Cardiothoracic Imaging 2020 2:3
20. Oudkerk M, Büller HR, Kuijpers D, et al. Diagnosis, Prevention, and Treatment of Thromboembolic Complications in COVID-19: Report of the National Institute for Public Health of the Netherlands. Radiology. 2020;201629.
21. Pulmonary Embolism on CTPA in COVID-19 Patients. Kaminetzky M, Moore W, Fansiwala K, Babb JS, Kaminetzky D, Horwitz LI, McGuinness G, Knoll A, and Ko JP. Radiology: Cardiothoracic Imaging. 2020 2:4.
22. Koike H, Sueyoshi E, Sakamoto I, Uetani M. Clinical Significance of Late Phase of Lung Perfusion Blood Volume (Lung Perfusion Blood Volume) Quantified by Dual-Energy Computed Tomography in Patients With Pulmonary Thromboembolism. J Thorac Imaging. 2017;32(1):43-49.
23. Qanadli SD, El Hajjam M, Vieillard-Baron A, et al. New CT index to quantify arterial obstruction in pulmonary embolism: comparison with angiographic index and echocardiography. AJR Am J Roentgenol. 2001;176(6):1415-1420.

24. Hansmann J, Apfaltrer P, Zoellner FG, et al. Correlation analysis of dual-energy CT iodine maps with quantitative pulmonary perfusion MRI. World J Radiol. 2013;5(5):202-207.
25. Boyden EA. “Segmental Anatomy of the Lungs” The British Journal of Surgery, 1954.
26. Hoey ET, Mirsadraee S, Pepke-Zaba J, Jenkins DP, Gopalan D, Screaton NJ. Dual-energy CT angiography for assessment of regional pulmonary perfusion in patients with chronic thromboembolic pulmonary hypertension: initial experience. AJR Am J Roentgenol. 2011;196(3):524-532.
27. Ameli-Renani S, Rahman F, Nair A, et al. Dual-energy CT for imaging of pulmonary hypertension: challenges and opportunities. Radiographics. 2014;34(7):1769-1790.
28. Thieme SF, Johnson TR, Lee C, et al. Dual-energy CT for the assessment of contrast material distribution in the pulmonary parenchyma. AJR Am J Roentgenol. 2009;193(1):144-149.
29. Syngo CT Dual Energy Indications For Use. Print No. C2-via-DE.621.01.02.02 Siemens Healthcare GmbH 2018.
30. Keir GJ, Nair A, Giannarou S, et al. Pulmonary vasospasm in systemic sclerosis: noninvasive techniques for detection. Pulm Circ. 2015;5(3):498-505.
31. Szekely Y, Lichter Y, Taieb P, et al. The Spectrum of Cardiac Manifestations in Coronavirus Disease 2019 (COVID-19) - a Systematic Echocardiographic Study. Circulation. 2020;10.1161.
32. Repessé X, Charron C, Vieillard-Baron A. Acute cor pulmonale in ARDS: rationale for protecting the right ventricle. Chest. 2015;147(1):259-265.
33. Fuld MK, Halaweish AF, Haynes SE, Divekar AA, Guo J, Hoffman EA. Pulmonary perfused blood volume with dual-energy CT as surrogate for pulmonary perfusion assessed with dynamic multidetector CT. Radiology. 2013;267(3):747-756.
34. Kay FU, Beraldo MA, Nakamura MAM, et al. Quantitative Dual-Energy Computed Tomography Predicts Regional Perfusion Heterogeneity in a Model of Acute Lung Injury. J Comput Assist Tomogr. 2018;42(6):866-872.
35. Chong PY, Chui P, Ling AE, et al. Analysis of deaths during the severe acute respiratory syndrome (SARS) epidemic in Singapore: challenges in determining a SARS diagnosis. Arch Pathol Lab Med. 2004;128(2):195-204.

36. Xiang-Hua Y, Le-Min W, Ai-Bin L, et al. Severe acute respiratory syndrome and venous thromboembolism in multiple organs. Am J Respir Crit Care Med. 2010;182(3):436-437.

Table 1: Demographic Patient Characteristics

Variable	Mean	SD
Age (years)	56.03	8.65
Height (m)	1.72	.06
Weight (kg)	84.10	17.02
Body mass index (BMI) kg/m^2	28.54	5.05
	N = 27	%
Male	20	74.1
Female	7	25.9
Diabetes	7	25.9
Hypertension	12	44.4
Repeat DECTPA	11	40.7
Ethnicity		
White	9	33.3
Asian	15	55.6
Black British or African	3	11.1
Clinical diagnosis, therapy and outcome		
Pulmonary embolism	11	40.7
Deep venous thrombosis	9	37.5

Therapeutic Enoxaparin	20	74.1
Prophylactic enoxaparin only	6	22.2
Unfractionated Heparin	4	11.1
Systemic thrombolysis	2	7.4
Outcome		
Discharge	21	77.8
Death	6	22.2

Table 2: Laboratory and Ventilatory Values at Time of DECTPA

Variable	Mean	SD	Normal range
Ferritin (ng/ml)	1122.04	1953.80	Males 20 - 250 Females 10 - 120
D-dimer (ng/ml)	5500.05	8691.15	<250
Lactate dehydrogenase (U/l)	782.08	329.50	140 - 280
Fibrinogen g/l	6.20	1.93	2-4
Pao2 (kPa)	9.09	1.40	10.5 - 13.5
Dynamic Compliance ml/cmH2O	32.9	19.1	50-100
PEEP (cm H_20)	10	2.7	

Table 3: Imaging Data (all DECTPA studies, n = 38)

Variable	Mean	SD	Range
Average perfusion defect %	36.1	17.2	10-77.5
Average PBV/PAenh	18.21	4.3	11.40-27.57
Average iodine density mg/ml	2.5	0.7	1.5-4.3
	Number	%	
Dose length product (mGy*cm)	247.97	113.40	112-626
Effective dose (mSv)	3.47	1.58	1.5-8.764

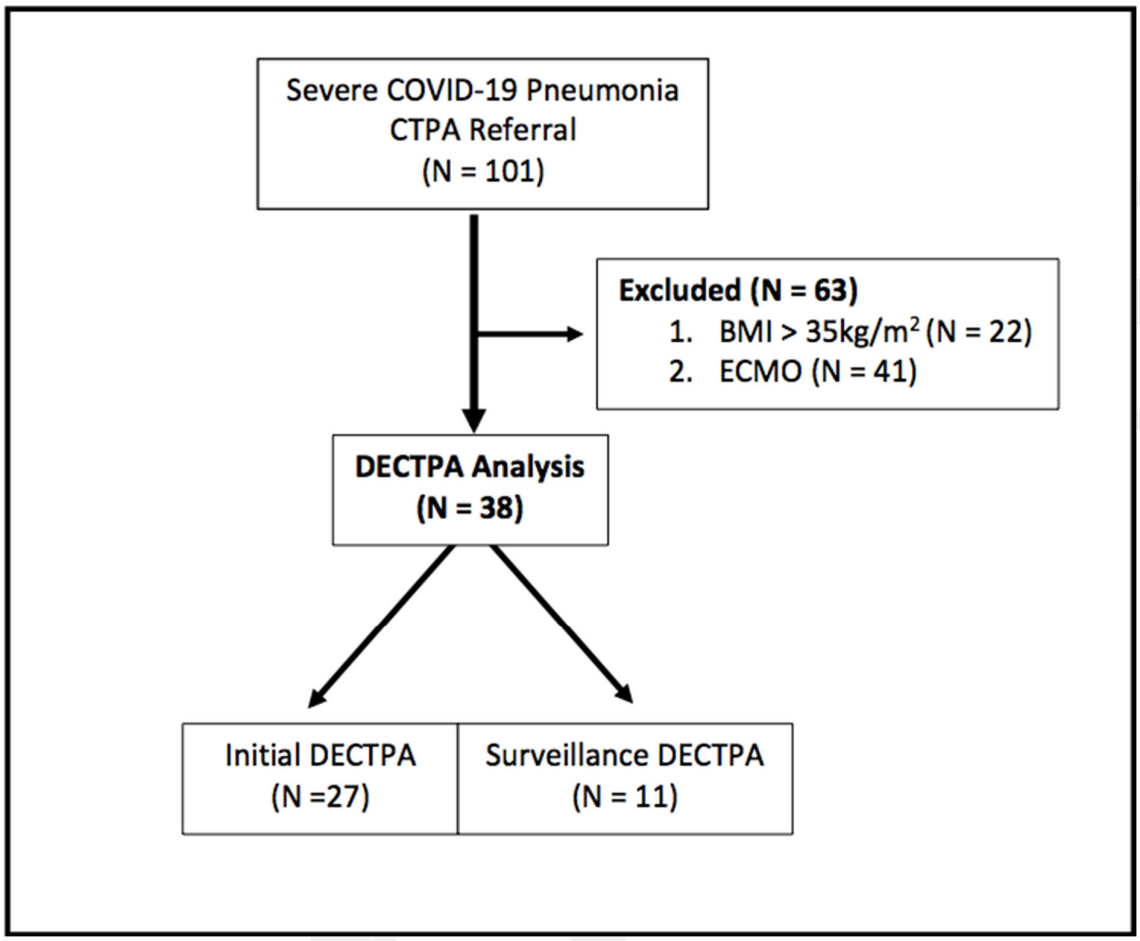

Figure 1: Flow diagram of patient inclusion for analysis.

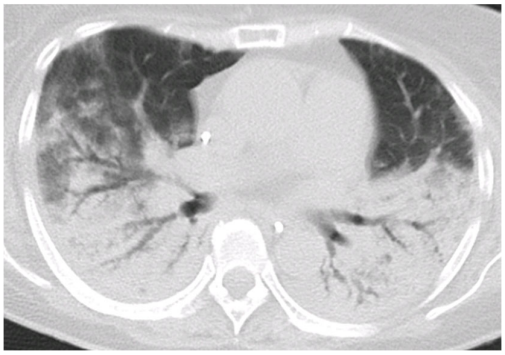

2A

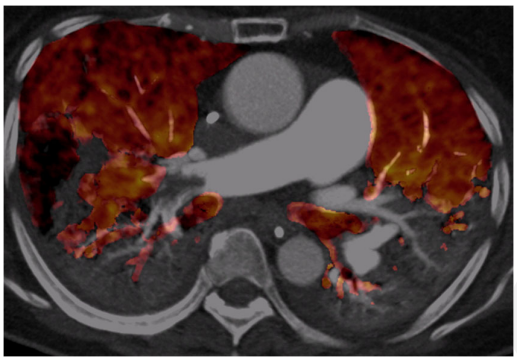

2B

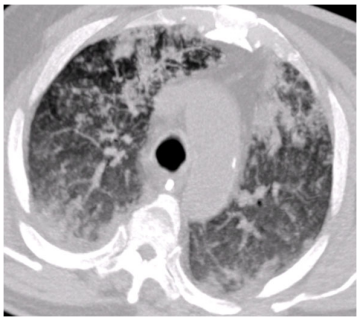

2C

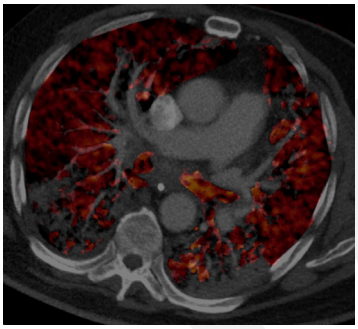

2D

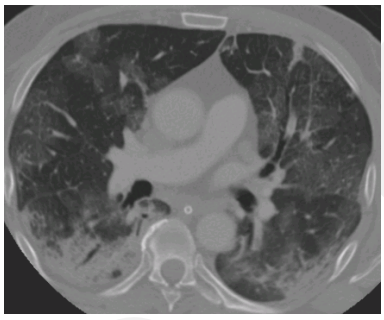

2E

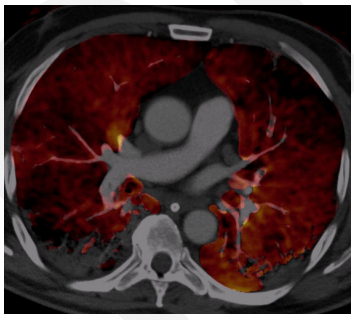

2F

Figure 2: Axial CT (A) and DECTPA PBV (B) images of a 61 –year-old female with severe COVID-19 pneumonia with worsening hypoxia 24 days after symptom onset. CT demonstrates a wedge-shaped defect in the right upper lobe, with associated ground glass opacity and a high attenuation rim, consistent with a pulmonary infarct and right pulmonary embolism. Additional findings include dense dependent consolidation with air bronchograms and antidependent ground glass opacity. Axial CT (C) and DECTPA PBV (D) images of a 58-year-old male with COVID-19 pneumonia imaged with DECTPA 10 days after symptom onset. Axial thick MIP images demonstrate small vessel enlargement manifesting as tree in bud nodules in the right upper lobe with corresponding mottled pattern perfusion

defects on the PBV colour map, with confluent ground glass opacity in all lobes. Axial CT (E) and DECTPA PBV (F) images of a 50-year-old male with severe COVID-19 pneumonia imaged 9 days after symptom onset, demonstrates extensive ground glass attenuation with interspersed normal aerated lung and amorphous perfusion defects on PBV maps which correspond with lucent and ground glass attenuation lung.

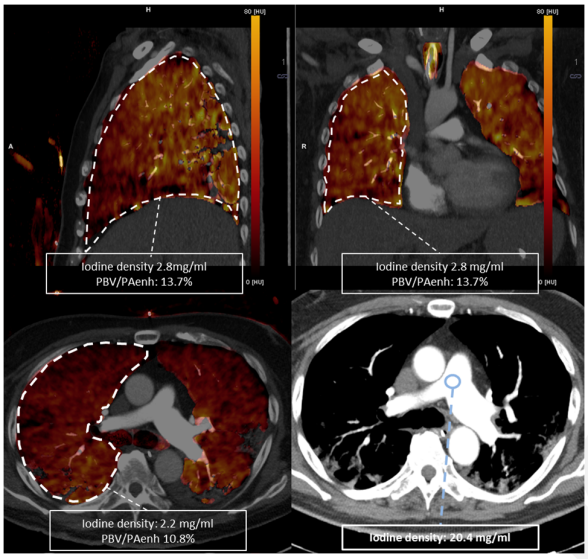

Figure 3: DECTPA in a 65 year old male 20 days after symptom onset. PBV maps were adjusted for pulmonary artery opacification by drawing a 1cm^2 region of interest (ROI) over the main pulmonary artery in transaxial section to quantify pulmonary artery enhancement (blue circle, bottom left). The mean "overlay value" of the ROI represents the calculated enhancement in HU within the parenchyma is acquired by manually tracing a ROI (dashed lines) around the perimeter of the right and left lungs in mid-sagittal (top left), mid-coronal (top right) and mid-axial (bottom left) planes. The RLE value for each ROI is the percentage enhancement of that ROI divided by pulmonary artery enhancement. Whole lung RLE was estimated as an average of these 6 measurements, the right lung measurements of this patient are shown for illustration.

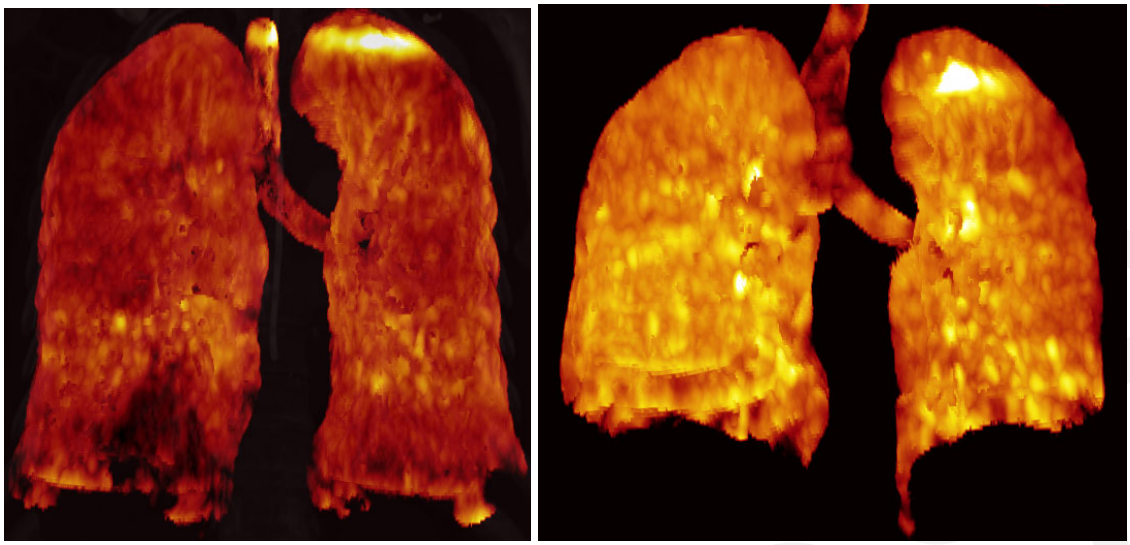

4A 4B

Figure 4: Thick maximal intensity projection (MIP) image of 62 year old female 19 and 38 days after symptom onset demonstrate initial globally reduced perfusion (mean RLE 11.4%), with a right lower lobe wedge shaped perfusion defect due to a segmental PE. The patient was then treated with anticoagulation and surveillance DECTPA demonstrated an improvement in global perfusion (mean RLE 20.6%) and resolution of the wedge shaped perfusion defect. The patient was self-ventilating through a tracheostomy at the time of this second study, accounting for lower lung volumes.

Supplementary data

Dual Energy CT Pulmonary Angiography Acquisition

All patients were scanned in a dedicated COVID-19 CT suite using a 2nd generation dual-source CT system (Somatom Definition Flash; Siemens Healthineers). DECTPA was part of the initial imaging assessment of all patients admitted with severe COVID-19 pneumonia to diagnose or exclude PE. CT images were acquired and perfusion maps generated, the latter using the dual-energy post-processing software, Syngo Via Dual Energy, Siemens Healthineers. Vendor recommended kVp settings for DECT were 100 and 140Sn kVp, Scanning parameters were as follows: quality reference mAs of 89 for 100 kVp and 76 for 140Sn kVp, 64 mm × 0.6 mm collimation with z-flying focal spot, 0.285 s rotation time, and pitch of 0.55. Images were reconstructed at 2 x 1.4 mm slice thickness using a dual-energy specific D30f kernel. Contrast volume was 70-100 ml of Omnipaque (Iohexol, GE Healthcare, Oslo, Norway) with an injection rate of 5 mL/s through a femoral or internal jugular central venous catheter or an 18G cannula in the antecubital vein. A triphasic contrast injection was employed, with 80% of the contrast administered without diluent, followed by 20% of the contrast volume in a 50:50 solution with normal saline, and a 20 cc normal saline chaser. Bolus tracking was used with a region of interest (ROI) on the main pulmonary artery.

All patients were imaged with their arms extended cranially in a caudocranial injection; 3 patients were imaged in the prone position to alleviate oxygen requirements. Dose length product (DLP) was recorded and effective dose was obtained by multiplying the mean DLP value by the adult chest k-factor of 0.014 mSv*mGy−1*cm−1.

Quantification of Morphologic CT Abnormalities

Two observers visually inspected for the following CT features:

i) Presence/absence of pulmonary arterial filling defect
ii) The ‘highest’ order of PE (1, main pulmonary artery; 2, right or left ; 3, lobar; 4, segmental and 5, subsegmental)

The incidence of venous thrombosis was documented using compression ultrasound and/or CT venography reports.

DECTPA Quantitative Measurement Definition (29):

PBV/PAenh (%): Ratio of iodine density in a manually selected region of interest relative to the iodine density in the main pulmonary artery (supplementary Figure 1).

Supplementary Table 1: Comparison of Quantitative DECTPA Parameters Between Study Cohort and Seven Normal Unmatched Volunteers (4 males, 3 females).

Variable	COVID+	Normal controls	P-value
Age	56.03	43.57	0.012
Height (m)	1.71	1.73	0.421
Weight (kg)	84.10	76.14	0.248
MPA attenuation (HU)	279.30	240.9	0.38
Average PBV/PAenh	18.21	27.05	0.002
Iodine Density (mg/ml)	2.5	2.47	0.7

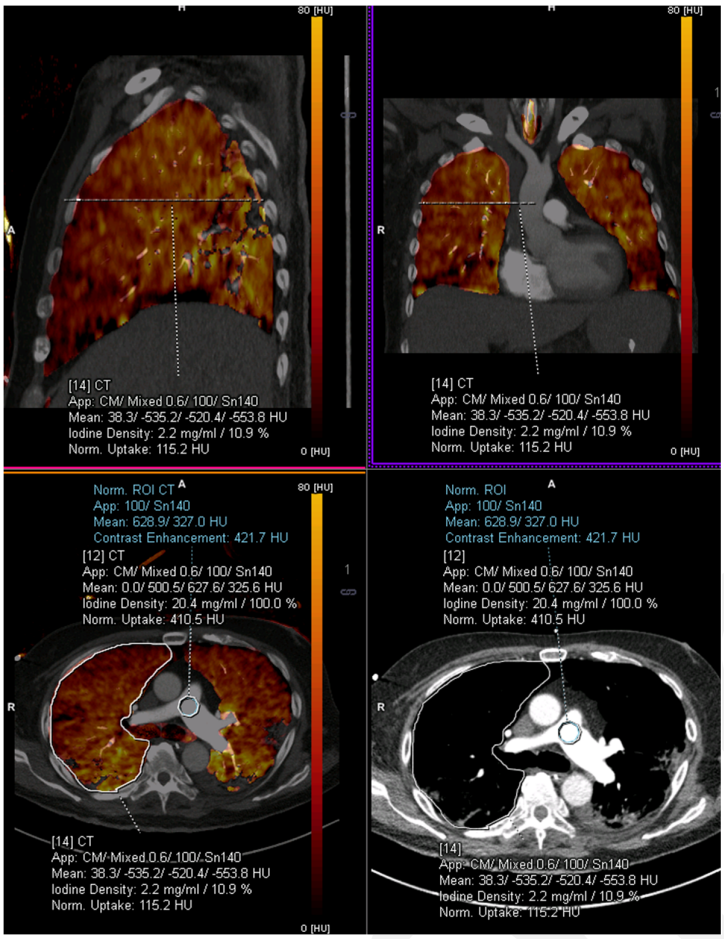

Supplementary Figure 1: DECTPA in a 65 year old male 20 days after symptom onset. PBV maps were adjusted for pulmonary artery opacification by drawing a 1cm^2 region of interest (ROI) over the main pulmonary artery in transaxial section (ROI 12, bottom left). The iodine distribution within the parenchyma was acquired by creating a ROI around the perimeter of the lungs in axial, sagittal and coronal planes, illustrated here as a white line around the right lung in the axial plane (ROI 14, bottom left). The iodine density of this ROI is 2.22 mg/ml, divided by the iodine density within the main pulmonary artery (20.44 mg/ml), this produces a PBV/PAenh of 10.9%.